ESTIMATION OF NONORTHOGONAL SHEAR WAVE POLARIZATIONS AND SHEAR WAVE VELOCITIES FROM FOUR-COMPONENT DIPOLE LOGS

Bertram Nolte and Arthur C. H. Cheng

Earth Resources Laboratory
Department of Earth, Atmospheric, and Planetary Sciences
Massachusetts Institute of Technology
Cambridge, MA 02139

ABSTRACT

Polarizations of split shear waves and flexural borehole waves are most commonly estimated from four-component data using the rotation technique of Alford (1986). This method is limited to the case of the two polarizations being orthogonal to each other. We present a method that is able to handle the case of nonorthogonally polarized waves and, moreover, is computationally more efficient than Alford's technique. Our method is based on the eigenvalue decomposition of an asymmetric matrix and a least-squares minimization of its off-diagonal components. In the case of orthogonally polarized waves, our method will yield exactly the same results as the Alford rotation. We apply our method to a cross-dipole shear-wave logging data set from the Powder River Basin in Wyoming and find that independently rotated source-receiver sets are very consistent with each other in anisotropic sections. After the rotation we compare two methods for estimating the phase velocities of fast and slow waves—a semblance method and homomorphic processing (Ellefsen *et al.*, 1993). We find homomorphic processing to be more reliable due to the dispersive nature of flexural waves.

INTRODUCTION

Both seismic shear waves and borehole flexural waves split into two independently propagating wave types when they travel through an anisotropic medium. The polarizations of these two wave types depend on the elastic properties of the medium. Therefore, if polarizations can be estimated from data, inferences can be made about the medium. In a wide variety of circumstances, anisotropy of the upper crust is believed to be caused by aligned cracks or fractures (e.g., Crampin, 1985). For wave propagation in a direction

parallel to such fractures, the faster split shear wave will be polarized parallel to the fractures and the slower shear wave will be polarized perpendicular to them.

Because polarization of shear waves can be an important indicator of fracture orientation, techniques for the estimation of the polarizations is a widely used step in shear wave and dipole-logging data processing. The most commonly used method is the rotation technique of Alford (1986), usually referred to as Alford rotation. This method rotates four-component data in small angle increments and computes the cross-component energy at each step. The polarization angles of the split shear waves are obtained as angles with minimal cross-component energies.

While this method works well in many circumstances it has two major drawbacks. First, it requires the two waves to be polarized orthogonally, which is true only for wave propagation in symmetry planes. Even though this assumption is valid in many cases, e.g., in cases where one set of aligned fractures is the only cause of anisotropy, it should not be made generalized. The second drawback of Alford rotation is that it requires the computation of many repeated rotations, which is computationally inefficient. Murtha (1988) addressed this problem and derived an analytic solution for the minimization of the cross-component energies. This solution, however, is only valid for the case of orthogonal polarization.

Several techniques have been proposed for polarization analysis of nonorthogonally split waves. One of these methods is the linear transform technique (Li and Crampin, 1993). In this method the particle motion is linearized in a point-by-point fashion and the polarization is estimated from the linearized motion. While this method is not restricted to orthogonal polarization, its performance has been less than satisfying (Tao *et al.*, 1995). The reason for this may be that the point-by-point linearization is a questionable strategy. Another rotation method is the dual-source independent source-geophone rotation technique (DIT) technique (Zeng and MacBeth, 1993). The difference between this method and the Alford rotation is that in DIT the rotation angles of the two rotations (one from the source to the principal directions and one from the principal directions to the receivers) may be different. These two rotations describe the case of the source dipoles not being aligned with the receivers, which will lead to an asymmetric data matrix. However, contrary to the authors' claim, the method does not apply to the case of nonorthogonal polarization.

We show here how Alford rotation can be extended to the case of nonorthogonally polarized waves. We also show how the minimization of the off-line energies can be performed efficiently without the need for repeated rotations. If the waves are orthogonally polarized, our method will yield exactly the same result as Alford rotation.

ROTATION TO NONORTHOGONAL PRINCIPAL DIRECTIONS

Let θ be the angle between one of the principal axis and the x-direction and let η be the angle by which the shear-wave (or flexural-wave) polarization deviates from orthogonality (see the appendix). If the source dipole is oriented in the x-direction the

components of the recorded wave field can be written as (see the appendix)

$$u_{xx}(t) = s(t) * p_1(t)\frac{\cos\theta\cos(\theta+\eta)}{\cos\eta} + s(t) * p_2(t)\frac{\sin\theta\sin(\theta+\eta)}{\cos\eta} \tag{1}$$

$$u_{yx}(t) = [-s(t) * p_1(t) + s(t) * p_2(t)]\frac{\sin\theta\cos(\theta+\eta)}{\cos\eta} \tag{2}$$

where u_{ik} denotes the wave field recorded on the i-component for a source oriented in the k-direction; $s(t)$ is the source signature, $p_1(t)$ and $p_2(t)$ are the medium responses in the two principle directions, and $*$ denotes convolution.

Similarly, the wavefields for the y-source are:

$$u_{xy}(t) = [-s(t) * p_1(t) + s(t) * p_2(t)]\frac{\cos\theta\sin(\theta+\eta)}{\cos\eta} \tag{3}$$

$$u_{yy}(t) = s(t) * p_1(t)\frac{\sin\theta\sin(\theta+\eta)}{\cos\eta} + s(t) * p_2(t)\frac{\cos\theta\cos(\theta+\eta)}{\cos\eta}. \tag{4}$$

We combine these four components in a matrix $\mathbf{U}$:

$$\mathbf{U}(t) = \begin{bmatrix} u_{xx}(t) & u_{xy}(t) \\ u_{yx}(t) & u_{yy}(t) \end{bmatrix}. \tag{5}$$

This matrix can be written as:

$$\mathbf{U}(t) = \mathbf{R}(\theta,\eta)\mathbf{D}(t)\mathbf{R}^{-1}(\theta,\eta) \tag{6}$$

with

$$\mathbf{D}(t) = \begin{bmatrix} s(t) * p_1(t) & 0 \\ 0 & s(t) * p_2(t) \end{bmatrix} \tag{7}$$

$$\mathbf{R}(\theta,\eta) = \begin{bmatrix} \cos\theta & \sin(\theta+\eta) \\ -\sin\theta & \cos(\theta+\eta) \end{bmatrix} \tag{8}$$

$$\mathbf{R}^{-1}(\theta,\eta) = \frac{1}{\cos\eta}\begin{bmatrix} \cos(\theta+\eta) & -\sin(\theta+\eta) \\ \sin\theta & cos\theta \end{bmatrix}. \tag{9}$$

Equation (6) is the eigenvalue decomposition of the asymmetric matrix $\mathbf{U}$. From this equation we obtain

$$\mathbf{D}(t) = \mathbf{R}^{-1}(\theta,\eta)\mathbf{U}(t)\mathbf{R}(\theta,\eta) \tag{10}$$

We now define matrix $\mathbf{D}'(t)$ as:

$$\mathbf{D}'(t) = \cos\eta\mathbf{D}(t) = \begin{bmatrix} s(t) * p_1(t)\cos\eta & 0 \\ 0 & s(t) * p_2(t)\cos\eta \end{bmatrix} \tag{11}$$

so that

$$\mathbf{D}'(t) = \begin{bmatrix} \cos(\theta+\eta) & -\sin(\theta+\eta) \\ \sin\theta & \cos\theta \end{bmatrix} \mathbf{U}(t) \begin{bmatrix} \cos\theta & \sin(\theta+\eta) \\ -\sin\theta & \cos(\theta+\eta) \end{bmatrix}. \tag{12}$$

This matrix should in theory be diagonal. We therefore want to find angles θ and η that minimize the components $d'_{xy}(t)$ and $d'_{yx}(t)$ in a least-squares sense over some time window. We write these components as vectors $\mathbf{d'_{xy}} = d'_{xy}(t)$ and $\mathbf{d'_{yx}} = d'_{yx}(t)$. The length of both these vectors is the number of time samples in the window. Thus, we will minimize the two terms

$$E_{xy} = \mathbf{d'_{xy}}^T \mathbf{d'_{xy}} \tag{13}$$

and

$$E_{yx} = \mathbf{d'_{yx}}^T \mathbf{d'_{yx}}. \tag{14}$$

From equation (12) we obtain:

$$\mathbf{d_{xy}} = \mathbf{u_{xy}} \cos^2(\theta+\eta) + \mathbf{u_{yx}} \sin^2(\theta+\eta) + (\mathbf{u_{xx}} - \mathbf{u_{yy}}) \cos(\theta+\eta)\sin(\theta+\eta) \tag{15}$$

and

$$\mathbf{d_{yx}} = \mathbf{u_{yx}} \cos^2\theta + \mathbf{u_{xy}} \sin^2\theta + (\mathbf{u_{xx}} - \mathbf{u_{yy}}) \cos\theta \sin\theta. \tag{16}$$

Equation (15) is a function of $\theta+\eta$ only, and equation (16) is a function of θ only. Thus both angles can be obtained separately. The angles are found by minimizing equations (13) and (14). In order to perform a computationally-efficient minimization, we need the derivatives of these equations with respect to the angles. Both equations (15) and (16) are of the form:

$$\mathbf{e} = \mathbf{a}\cos^2\phi + \mathbf{b}\sin^2\phi + \mathbf{c}\cos\phi\sin\phi. \tag{17}$$

We thus need the derivative of terms of the form $\mathbf{e}^T\mathbf{e}$. The first and second derivatives are

$$\begin{aligned} \frac{d(\mathbf{e}^T\mathbf{e})}{d\phi} &= 2(\mathbf{a}^T\mathbf{c}\cos^4\phi + (2\mathbf{a}^T\mathbf{b} - 2\mathbf{a}^T\mathbf{a} + \mathbf{c}^T\mathbf{c})\cos^3\phi\sin\phi \\ &\quad +(3\mathbf{b}^T\mathbf{c} - 3\mathbf{a}^T\mathbf{c})\cos^2\phi\sin^2\phi + \\ &\quad (-2\mathbf{a}^T\mathbf{b} + 2\mathbf{b}^T\mathbf{b} - \mathbf{c}^T\mathbf{c})\sin^3\phi\cos\phi - \mathbf{b}^T\mathbf{c}\sin^4\phi) \end{aligned} \tag{18}$$

$$\begin{aligned} \frac{d^2(\mathbf{e}^T\mathbf{e})}{d\phi^2} &= 2((2\mathbf{a}^T\mathbf{b} - 2\mathbf{a}^T\mathbf{a} + \mathbf{c}^T\mathbf{c})\cos^4\phi \\ &\quad +(-4\mathbf{a}^T\mathbf{c} + 6\mathbf{b}^T\mathbf{c} - 6\mathbf{a}^T\mathbf{c})\cos^3\phi\sin\phi \\ &\quad +(-12\mathbf{a}^T\mathbf{b} + 6\mathbf{a}^T\mathbf{a} + 6\mathbf{b}^T\mathbf{b} - 6\mathbf{c}^T\mathbf{c})\cos^2\phi\sin^2\phi \\ &\quad +(-4\mathbf{b}^T\mathbf{c} - 6\mathbf{b}^T\mathbf{c} + 6\mathbf{a}^T\mathbf{c})\sin^3\phi\cos\phi \\ &\quad +(2\mathbf{a}^T\mathbf{b} - 2\mathbf{b}^T\mathbf{b} + \mathbf{c}^T\mathbf{c})\sin^4\phi). \end{aligned} \tag{19}$$

Since both the first and the second derivatives are available, the minimum of $\mathbf{e}^T\mathbf{e}$ can be computed easily. For example, we can use a Newton method, i.e., solve the iterative equation

$$\phi_{i+1} = \phi_i - \left[\frac{d(\mathbf{e}^T\mathbf{e})}{d\phi} \Big/ \frac{d^2(\mathbf{e}^T\mathbf{e})}{d\phi^2} \right]_{\phi=\phi_i} . \tag{20}$$

Equation (20) converges rapidly so that only a few iterations are needed. If a maximum is found instead of a minimum, a new search starting at an angle 45° away from the maximum will converge to the minimum. Once the minimum is found for one cross-component, its value of ϕ can be used as a starting point in the search for the minimum of the other cross-component.

After both angles θ and $\theta + \eta$ have been found, we rotate the recordings to the principal direction using equation (10).

RELATION TO ALFORD ROTATION

We will now briefly show how the the eigenvector decomposition discussed above relates to Alford rotation, a method that rotates four-component data from an orthogonal coordinate system $\{x, y\}$ to a new system $\{x', y'\}$ which is also orthogonal.

We show how this rotation is performed in the case of nonorthogonal principal directions. In other words, we have to find $\mathbf{U}(\alpha, \eta)$ for some angle α given the measured $\mathbf{U}(\theta, \eta)$. For simplicity we will not explicitly write the time dependency of $\mathbf{U}$ and $\mathbf{D}$ in this section.

First, we write $\mathbf{R}$ in equation(8) as

$$\mathbf{R}(\theta, \eta) = \mathbf{W}(\theta)\mathbf{V}(\eta) \tag{21}$$

with

$$\mathbf{W}(\theta) = \begin{bmatrix} \cos\theta & \sin\theta \\ -\sin\theta & \cos\theta \end{bmatrix} \tag{22}$$

and

$$\mathbf{V}(\eta) = \begin{bmatrix} 1 & \sin\eta \\ 0 & \cos\eta \end{bmatrix} . \tag{23}$$

The matrix $\mathbf{W}$ is unitary ($\mathbf{W}^{-1} = \mathbf{W}^T$). Thus $\mathbf{R}^{-1}$ can be written as:

$$\mathbf{R}^{-1}(\theta, \eta) = \mathbf{V}^{-1}(\eta)\mathbf{W}^T(\theta) \tag{24}$$

with

$$\mathbf{V}^{-1}(\theta) = \begin{bmatrix} 1 & -\tan\eta \\ 0 & 1/\cos\eta \end{bmatrix} . \tag{25}$$

From equations (6), (21), and (24) we obtain

$$\mathbf{U}(\theta,\eta) = \mathbf{W}(\theta)\mathbf{V}(\eta)\mathbf{D}\mathbf{V}^{-1}(\eta)\mathbf{W}^T(\theta) \tag{26}$$

or

$$\mathbf{D} = \mathbf{V}^{-1}(\eta)\mathbf{W}^T(\theta)\mathbf{U}(\theta,\eta)\mathbf{W}(\theta)\mathbf{V}(\eta). \tag{27}$$

For any angle α the wave field is:

$$\mathbf{U}(\alpha,\eta) = \mathbf{W}(\alpha)\mathbf{V}(\eta)\mathbf{D}\mathbf{V}^{-1}(\eta)\mathbf{W}^T(\alpha) \tag{28}$$

From equations (27) and (28) we thus obtain

$$\mathbf{U}(\alpha,\eta) = \mathbf{W}(\alpha)\mathbf{W}^T(\theta)\mathbf{U}(\theta,\eta)\mathbf{W}(\theta)\mathbf{W}^T(\alpha) \tag{29}$$

or

$$\mathbf{U}(\alpha,\eta) = \mathbf{W}(\alpha-\theta)\mathbf{U}(\theta,\eta)\mathbf{W}^T(\alpha-\theta). \tag{30}$$

Equation (30) is the equation for Alford rotation. We have thus shown that $\mathbf{U}$ can be rotated in the same way as in the case of orthogonally-polarized waves. However, since x- and y-components of $\mathbf{U}(\alpha,\eta)$ are orthogonal, the rotation described in equation (30) cannot yield the principal time series if the polarizations are not orthogonal.

The Alford rotation technique searches for the angle that minimizes the cross-component energies. Writing $\phi = \alpha - \theta$, $\mathbf{U}' = \mathbf{U}(\alpha,\eta)$ and $\mathbf{U} = \mathbf{U}(\theta,\eta)$ the cross-components in equation (30) are

$$u'_{xy} = u_{xy}\cos^2(\phi) + u_{yx}\sin^2(\phi) + (u_{xx} - u_{yy})\cos(\phi)\sin(\phi) \tag{31}$$

$$u'_{yx} = u_{yx}\cos^2(\phi) + u_{xy}\sin^2(\phi) + (u_{xx} - u_{yy})\cos(\phi)\sin(\phi). \tag{32}$$

Comparing with equations (15) and (16) shows that the cross-component energies will have their minima exactly at θ and $\theta + \eta$, respectively. Thus, these angles could potentially also be found by Alford rotation, even though this would be computationally inefficient, thus solving equation (20) is preferable. Even if Alford rotation were used to find the angles, rotation to the principal directions still has to be performed using equation (10).

CORRECTION FOR TOOL ROTATION FOR DIPOLE LOGGING DATA

The Schlumberger dipole tool has two sources which are spaced 0.152 m (0.5 ft) apart from each other. If data are collected with this tool the components for the x-source are not exactly aligned with those of the y-source for the following reason: When one source is fired at some depth the tool has moved by 0.152 m from the position it was in when the other source was fired at the same depth. This movement is usually accompanied

by a rotation by some angle γ. Before we determine the polarizations we should correct for this effect.

Taking the rotation by γ into account leaves equations (1) and (2) unchanged, but in equations (3) and (4) θ is replaced by $\theta + \gamma$. These equations thus become

$$u_{xy}(t) = [-s(t) * p_1(t) + s(t) * p_2(t)] \frac{\cos(\theta+\gamma)\sin(\theta+\eta+\gamma)}{\cos\eta} \tag{33}$$

and

$$u_{yy}(t) = s(t)*p_1(t)\frac{\sin(\theta+\gamma)\sin(\theta+\eta+\gamma)}{\cos\eta} + s(t)*p_2(t)\frac{\cos(\theta+\gamma)\cos(\theta+\eta+\gamma)}{\cos\eta} \tag{34}$$

The components for the x-source [equations (1) and (2)] can be written as

$$\begin{bmatrix} u_{xx} \\ u_{yx} \end{bmatrix} = \mathbf{R}(\theta,\eta)\mathbf{D}(t)\mathbf{R}^{-1}(\theta,\eta) \begin{bmatrix} 1 \\ 0 \end{bmatrix} \tag{35}$$

and the components for the y-source [equations (33) and (34)] are now

$$\begin{bmatrix} u_{xy} \\ u_{yy} \end{bmatrix} = \mathbf{R}(\theta+\gamma,\eta)\mathbf{D}(t)\mathbf{R}^{-1}(\theta+\gamma,\eta) \begin{bmatrix} 0 \\ 1 \end{bmatrix}. \tag{36}$$

We now write

$$\mathbf{R}(\theta+\gamma,\eta) = \mathbf{S}(\gamma)\mathbf{R}(\theta,\eta) \tag{37}$$

with

$$\mathbf{S}(\gamma) = \begin{bmatrix} \cos\gamma & \sin\gamma \\ -\sin\gamma & \cos\gamma \end{bmatrix}. \tag{38}$$

The matrix $\mathbf{S}$ is unitary. Therefore we can write equation (36) as

$$\begin{bmatrix} u_{xy} \\ u_{yy} \end{bmatrix} = \mathbf{S}(\gamma)\mathbf{R}(\theta,\eta)\mathbf{D}(t)\mathbf{R}^{-1}(\theta,\eta)\mathbf{S}^T(\gamma) \begin{bmatrix} 0 \\ 1 \end{bmatrix} \tag{39}$$

or

$$\mathbf{S}^T(\gamma) \begin{bmatrix} u_{xy} \\ u_{yy} \end{bmatrix} = \mathbf{R}(\theta,\eta)\mathbf{D}(t)\mathbf{R}^{-1}(\theta,\eta) \begin{bmatrix} -\sin\gamma \\ \cos\gamma \end{bmatrix}. \tag{40}$$

Equations (35) and (40) can be combined as

$$\left[\begin{bmatrix} u_{xx} \\ u_{yx} \end{bmatrix}, \mathbf{S}^T \begin{bmatrix} u_{xy} \\ u_{yy} \end{bmatrix} \right] = \mathbf{R}(\theta,\eta)\mathbf{D}(t)\mathbf{R}^{-1}(\theta,\eta)\mathbf{T}(\gamma) \tag{41}$$

with

$$\mathbf{T}(\gamma) = \begin{bmatrix} 1 & -\sin\gamma \\ 0 & \cos\gamma \end{bmatrix}. \tag{42}$$

Finally, we obtain

$$\mathbf{U}' = \mathbf{T}^{-1}(\gamma)\left[\begin{bmatrix} u_{xx} \\ u_{yx} \end{bmatrix}, \mathbf{S}^T \begin{bmatrix} u_{xy} \\ u_{yy} \end{bmatrix}\right] = \mathbf{R}(\theta,\eta)\mathbf{D}(t)\mathbf{R}^{-1}(\theta,\eta) \tag{43}$$

with

$$\mathbf{T}^{-1} = \begin{bmatrix} 1 & \tan\gamma \\ 0 & 1/\cos\gamma \end{bmatrix}. \tag{44}$$

Equation (43) shows that the transformed matrix $\mathbf{U}'$ has the desired eigenvector composition.

EXAMPLE OF AN ASYMMETRIC DATA MATRIX

Figure 1 shows an example of an asymmetric data matrix. It is part of the same data set that is described in more detail below. Figure 1a shows the cross-component energies as a function angle. The three curves represent the two cross-component energies E_{xy} (solid) and E_{yx} (dashed) as well as their sum $E_{xy} + E_{yx}$ (dotted) which is the quantity that is usually minimized in Alford rotation. It is apparent in Figure 1a that the energy minima of the two components do not coincide; they are different by $\sim 18°$. Data-matrix asymmetry, as seen in this example, may have causes other than nonorthogonal polarization (MacBeth *et al.*, 1994). In any case, it is interesting to apply our nonorthogonal rotation algorithm to this example. The first arrivals on the in-line and off-line components after Alford rotation (rotation to the minimum of $E_{xy} + E_{yx}$) and after nonorthogonal rotation are shown on Figures 1b and 1c, respectively. Note that scales in Figures 1b and 1c are different. It can be seen clearly that the off-line amplitudes after the nonorthogonal rotation (solid) are smaller than the off-line amplitudes after Alford rotation (dashed). The in-line components are approximately the same in both cases. In this example, the energy ratio $E_{off-line}/E_{in-line}$ is 2.1% after Alford rotation and 0.9% after nonorthogonal rotation. This demonstrates that our method performs significantly better than Alford rotation in reducing off-line energy when the data matrix is asymmetric.

RESULTS

We now apply our rotation method to a dipole-logging data set from ARCO's Red Mountain Well in the Powder River Basin in Wyoming. Our data are from a depth interval of 152 m (500 ft) that includes the Niobrara formation at the top and the Frontier formation at the bottom. There is independent information (FMI/FMS) that both of these formations are fractures. We thus expect to see effects of anisotropy.

Figures 2a–d show the results for the 152 m (500 ft) depth interval. Data from every 10th shot are shown. Panel (a) shows the estimates for the polarization of the fast flexural wave for all receivers. Panel (b) shows the average polarization of the fast

wave (solid line) and the average polarization of the slow wave minus 90° (dashed line). Panel (c) shows the standard deviation at each source depth for both the fast (solid line) and the slow wave (dashed line). Panel (d) shows the time delay between fast and slow waves per distance traveled. The time delays were obtained by cross-correlation of the first arrivals on the principal components.

Figure 2 shows some striking differences between the two formations. The Frontier formation (depth below ~3.5 km) shows pronounced azimuthal anisotropy. The polarizations in this formation are consistent for all receivers, which is apparent in panel (a) and also in (c), which shows a low standard variation for this region. Moreover, the time delays (d) are pronounced for this region. The average polarization (b) varies between $\sim 60°$ and $\sim 100°$. As the anisotropy is most likely caused by vertical fractures these angles correspond to the strike of these fractures. In the Niobrara formation, on the other hand, the polarizations are less consistent and the time delays are generally smaller. However, there are several regions in which the polarizations are consistent among the different receivers. In those regions the average polarization of the fast shear wave is similar to the polarization in the Frontier formation.

Figure 3 shows the Frontier formation in more detail. Here every source depth is plotted. Panel (a) shows the mean values of polarization of the fast (solid line) and the slow flexural wave minus 90° (dashed line). The difference between these two polarizations is small (within the intervals given by the standard deviations). From this we can conclude that the split waves are in fact polarized orthogonally, as expected for anisotropy caused by aligned fractures. Within this depth interval the azimuth of the fast polarization varies by as much as 40°. The biggest change occurs in the depth interval between ~3.523 km and ~3.528 km where the polarization changes from $\sim 100°$ to $\sim 60°$. Note that what appears to be a gradual change in polarization might in reality be an abrupt change, as depth resolution is limited by the tool length. The time delay (panel b) reaches its maximum at a depth of ~3.525 km and drops drastically at slightly higher depths. Part of the reason for this behavior may be the polarization change that occurs at this depth. A wave that starts out as a fast wave at the source dipole will not be polarized in the fast direction when it reaches the receiver when the tool is crossing the transition.

Figure 4 shows an example of the data recorded by the dipole tool rotation to the principal directions. The data in Figure 4 are from a source depth of 3.525 km, i.e., from the depth of maximum anisotropy. The seismograms on the fast and slow components are displayed as solid and dashed lines, respectively. There is a pronounced time delay between the fast and the slow flexural waves in this example.

The next processing step is the estimation of the phase velocities of both wave types from the rotated data. A standard way to determine phase velocities from array data is to use a semblance method. The inherent problem with this method is that it cannot correctly handle the effects of dispersion and thus yields a result that can be at most approximately true. A method that allows for dispersion is homomorphic processing (Ellefsen *et al.*, 1993). This technique operates in the frequency domain and yields the

phase velocity as a function of frequency.

Figures 5a and 5b show two independent estimates of the phase velocities computed with these two methods. The velocities in (a) have been obtained with a semblance method. For the computation of the semblance we used a window that was 1.2 ms (30 samples) long. This window was moved over a time interval from 1.4 ms to 1.88 ms, which includes the first arrival in all traces. The semblance was computed for slowness steps of 6.56 μs/m (2 μs/ft). The velocities in (b) were obtained with homomorphic processing at a frequency of 2.93 Hz, which is the lowest frequency at which the SN-Ratio is high enough to reliably determine the velocities of both wave types.

Even though there is a rough agreement between both estimates there are also some pronounced differences. For example, at a depth of ~3.524 km the velocity of the fast wave that is obtained with homomorphic processing is significantly higher than the velocity obtained with the semblance method. The differences between the two measurements can be attributed to several effects. As mentioned, the semblance estimates do not allow for dispersion. The homomorphic processing, on the other hand, is quite sensitive to the window applied in the time domain before Fourier-transforming the data. Also, homomorphic processing involves unwrapping the phase of the signal recorded at each receiver. This step is another potential source of errors, because this step cannot always be performed unambiguously for noisy data. Clearly, both methods used for velocity estimation have their drawbacks and further research is needed in the field of estimating velocities for dispersive flexural waves.

CONCLUSIONS

We have presented a method of rotating four-component data to nonorthogonal principal directions and have derived its relation to Alford rotation. We have also shown how to correct for the effect of tool rotation between the recordings for the two source dipoles. When applied to a cross-dipole data set, our rotation method yielded consistent polarization azimuths for different source-receiver sets in anisotropic sections.

We then estimated the phase velocities on the principal components independently in two different ways—semblance and homomorphic processing. Even though there is a rough agreement between both results there are some notable differences. We believe that the results of homomorphic processing are more reliable, because they take into account the dispersive nature of flexural waves.

Generally, we find that it is easy to obtain reliable estimates of polarization angles from dipole logs, whereas estimating velocities is a more difficult problem that needs further research.

ACKNOWLEDGMENTS

We thank Keith Katahara of ARCO Oil and Gas Company for providing the data. This work was supported by the Borehole Acoustics and Logging Consortium at the Massachusetts Institute of Technology and by Department of Energy contract #DE-FG02-86ER13636.

REFERENCES

Alford, R. M., 1986, Shear data in the presence of azimuthal anisotropy, *56th Ann. Int. Mtg., Soc. Eplor. Geophys., Expanded Abstracts*, 476–479.

Crampin, S., 1985. Evaluation of anisotropy by shear-wave splitting, *Geophysics, 50*, 142–152.

Ellefsen, K.J., Burns, D.R., and Cheng, C.H., 1993, Homomorphic processing of the tube wave generated during acoustic logging, *Geophysics, 58*, 1400–1407.

Ellefsen, K.J., Cheng, C.H., and Toksöz, M.N., 1991, Effects of anisotropy upon the normal modes in a borehole, *J. Acoust. Soc. Am., 89*, 2597–2616.

Li, X.-Y. and Crampin, S., 1993, Linear-transform techniques for processing shear-wave anisotropy in four-component seismic data, *Geophysics, 58*, 240–256.

MacBeth, C., Zeng, X., Yardley, G.S., and Crampin, S, 1994, Interpreting data matrix asymmetry in near-offset shear-wave VSP data, *Geophysics, 59*, 176–191.

Murtha, P.E., 1988, Estimation of the rotation transformation angle for shear wave data acquired in azimuthally anisotropic regions, Abstract, *Third Int. Workshop on Seismic Anisotropy*, Berkeley, California.

Tao, G., Zhu, Z., and Cheng, C.H., 1995, An investigation on azimuthal anisotropy measurements with ultrasonic dipole data., *65th Ann. Int. Mtg., Soc. Eplor. Geophys., Expanded Abstracts*, 85–88.

Zeng, X. and MacBeth, C., 1993, Algebraic processing techniques for estimating shear-wave splitting in near-offset VSP data: Theory, *Geophys. Prosp., 41*, 1033–1066.

APPENDIX

Derivation of Equations (1) and (2)

Figure A-1a shows the projections of an x-source and a y-source onto the principal directions $\hat{p}_1$ and $\hat{p}_2$. By the law of sines we obtain for the projections of the x-source:

$$s_1 = s_x \frac{\sin(\delta - \theta)}{\sin(\pi - \delta)} = s_x \frac{\cos(\theta + \eta)}{\cos \eta} \tag{A-1}$$

$$s_2 = s_x \frac{\sin \theta}{\sin(\pi - \delta)} = s_x \frac{\sin \theta}{\cos \eta}. \tag{A-2}$$

The angles in equations (A-1) and (A-2) are defined in the figure.

Figure A-1b shows the projection of vectors r_1 and r_2 on the principal axes onto the x- and y-axes.

$$r_x = r_1 \cos \theta + r_2 \cos(\delta - \theta) = r_1 \cos \theta + r_2 \sin(\theta + \eta) \tag{A-3}$$

$$r_y = -r_1 \sin \theta + r_2 \sin(\delta - \theta) = -r_1 \sin \theta + r_2 \cos(\theta + \eta). \tag{A-4}$$

Substitution of (A-1) and (A-2) into (A-3) and using $s_x = s(t)$, $r_1(t) = p_1(t) * s_1(t)$, and $r_x = u_{xx}$ gives equation (1). Analogously, substitution of (A-1) and (A-2) into (A-4) with $r_y = u_{yx}$ gives equation (2).

Derivation of Equations (3) and (4)

Using the law of sines again, we obtain from Figure A-1a for the projections of a y-source onto the principal directions $\hat{p}_1$ and $\hat{p}_2$

$$s_1 = -s_y \frac{\sin(\theta + \eta)}{\cos \eta} \tag{A-5}$$

$$s_2 = s_y \frac{\cos \theta}{\cos \eta}. \tag{A-6}$$

Substitution of (A-5) and (A-6) into (A-3) and using $s_y = s(t)$, $r_1(t) = p_1(t) * s_1(t)$, and $r_x = u_{xy}$ gives equation (3). Analogously, substitution of (A-5) and (A-6) into (A-4) with $r_y = u_{yy}$ gives equation (4).

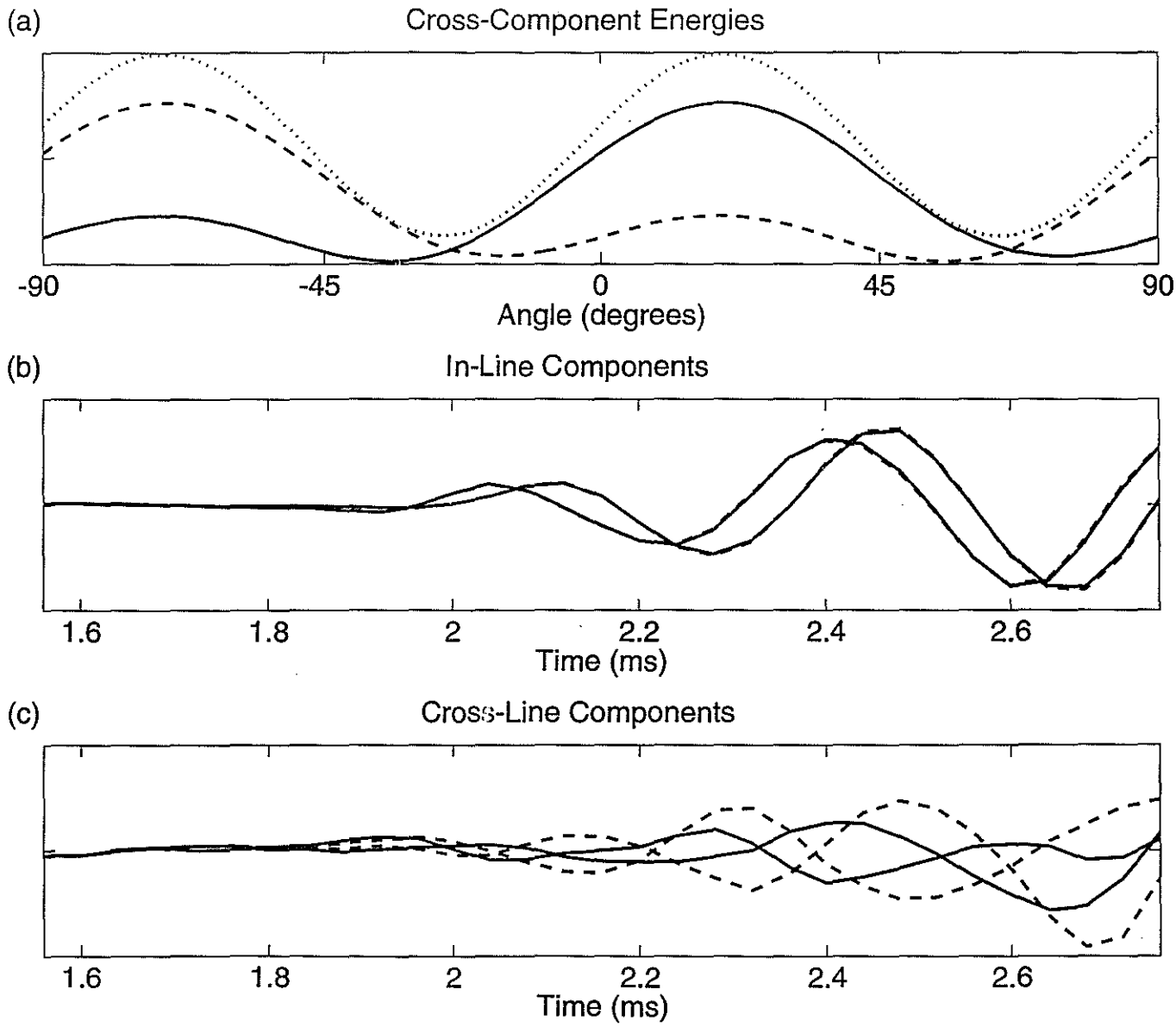

Figure 1: (a) Energies on the xy-component (solid) and the yx-component (dashed); sum of both energies (dotted); (b) in-line components after non-orthogonal rotation (solid) and Alford rotation (dashed); (c) cross-line components after non-orthogonal rotation (solid) and Alford rotation (dashed).

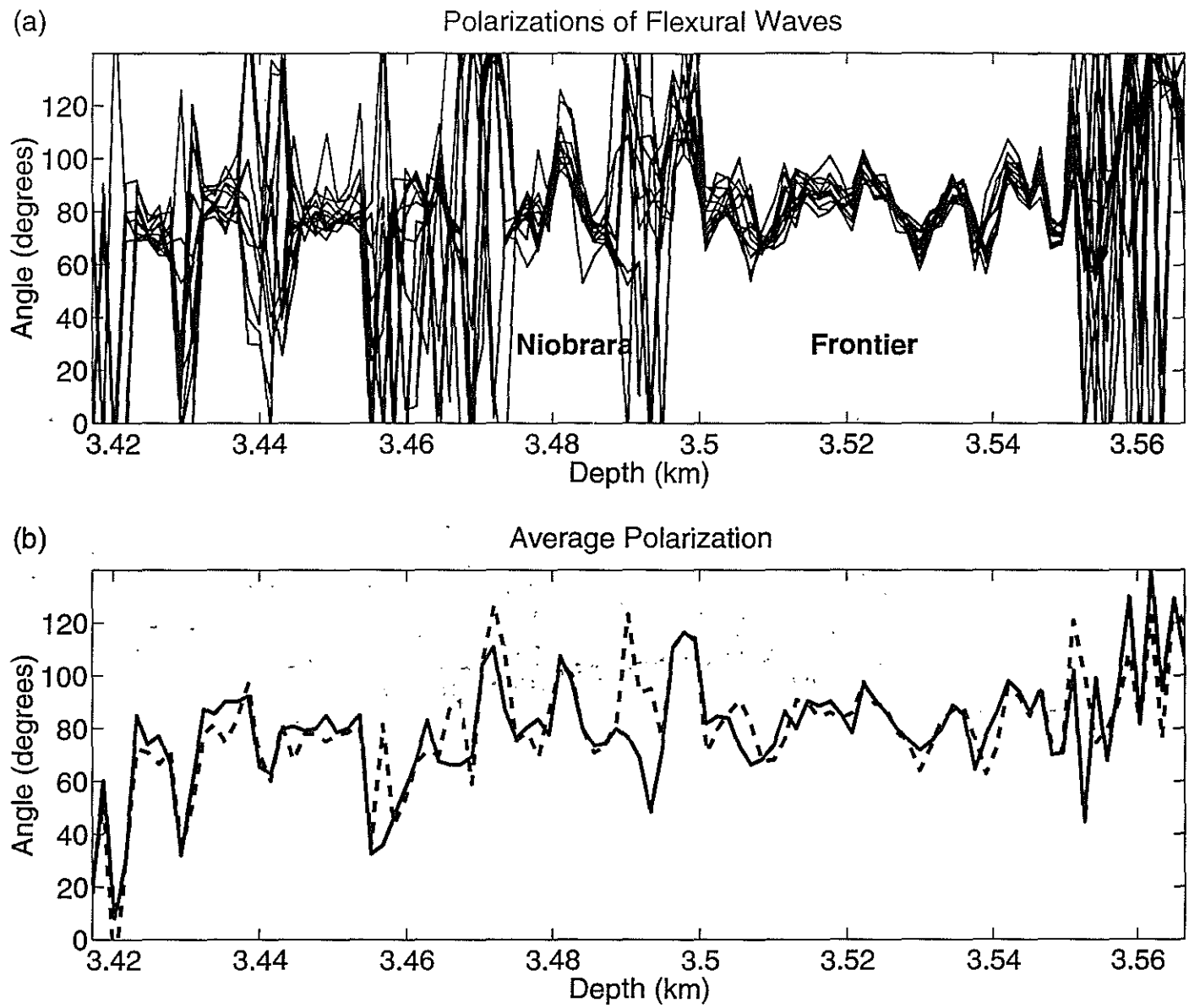

Figure 2: Niobrara and Frontier formations: (a) Polarizations of fast flexural waves and polarizations of slow flexural waves minus 90° for each receiver; (b) average values of the polarization of the fast wave (solid) and the polarization of the slow wave minus 90° (dashed).

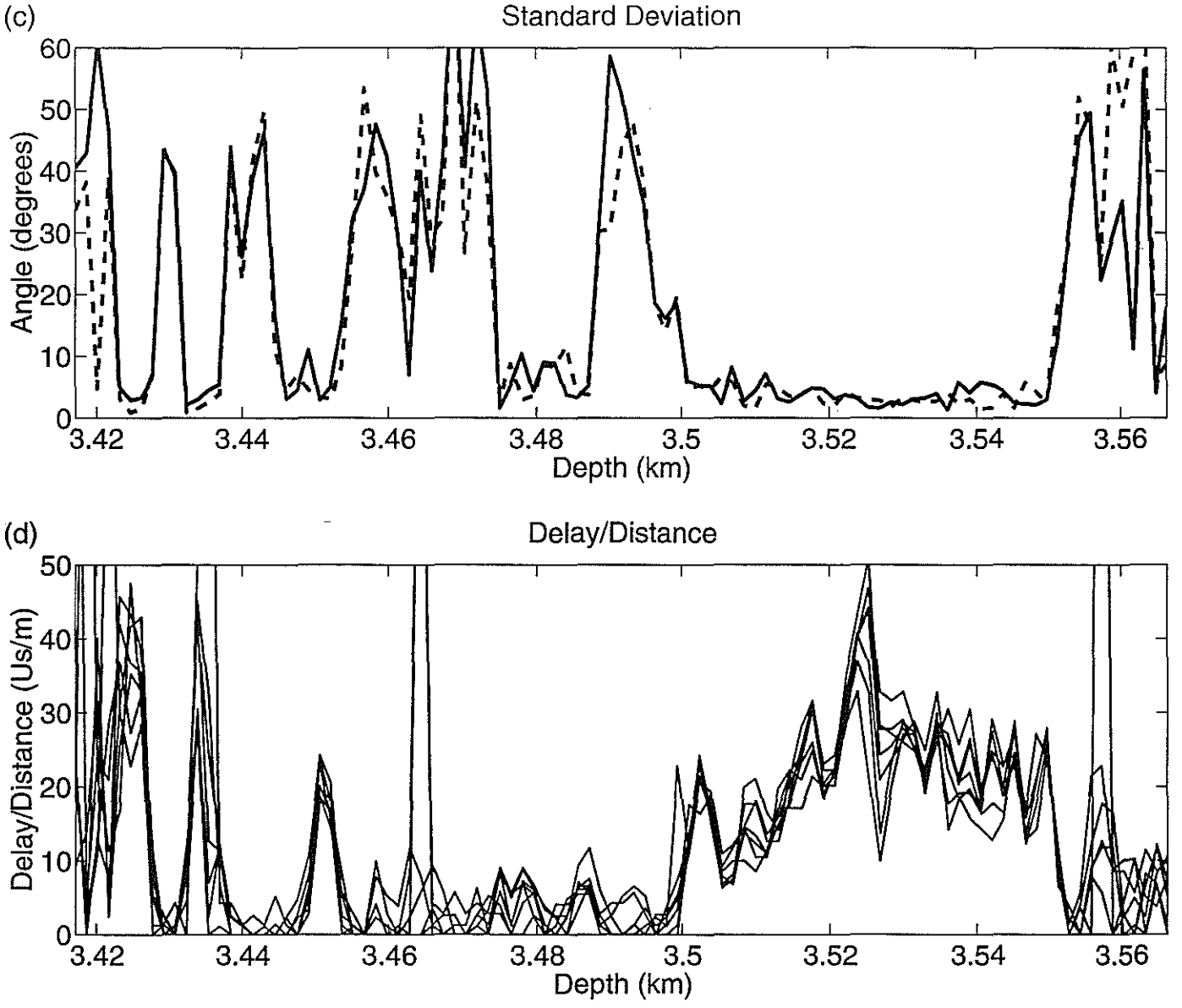

Figure 2, ctd.: (c) Standard deviations of fast (solid) and slow (dashed) polarizations; (d) time delay between fast and slow waves per distance traveled.

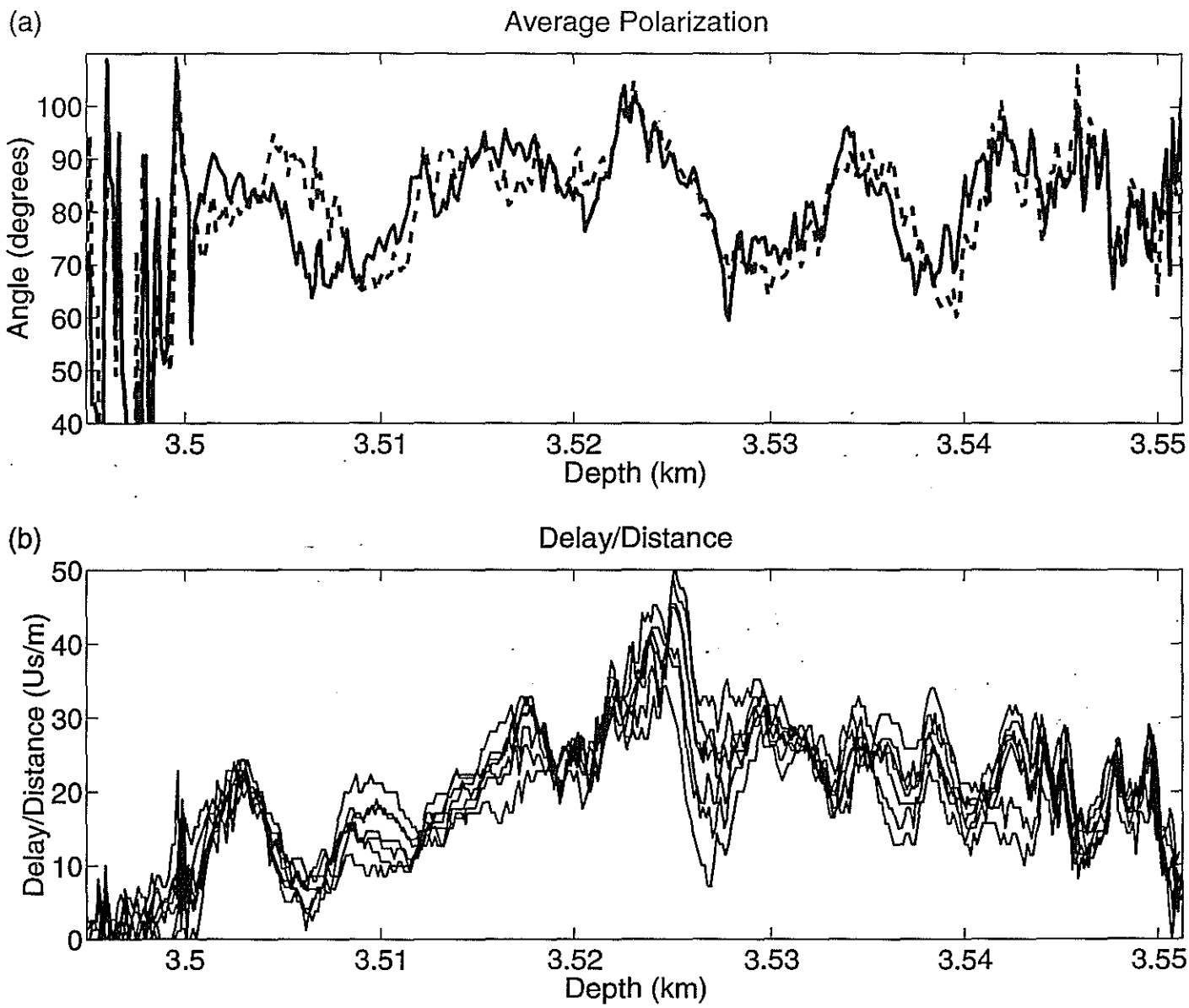

Figure 3: Frontier formation: (a) Average polarization of fast wave (solid) and average polarization of slow wave minus 90° (dashed); (b) time delay between fast and slow waves per distance traveled.

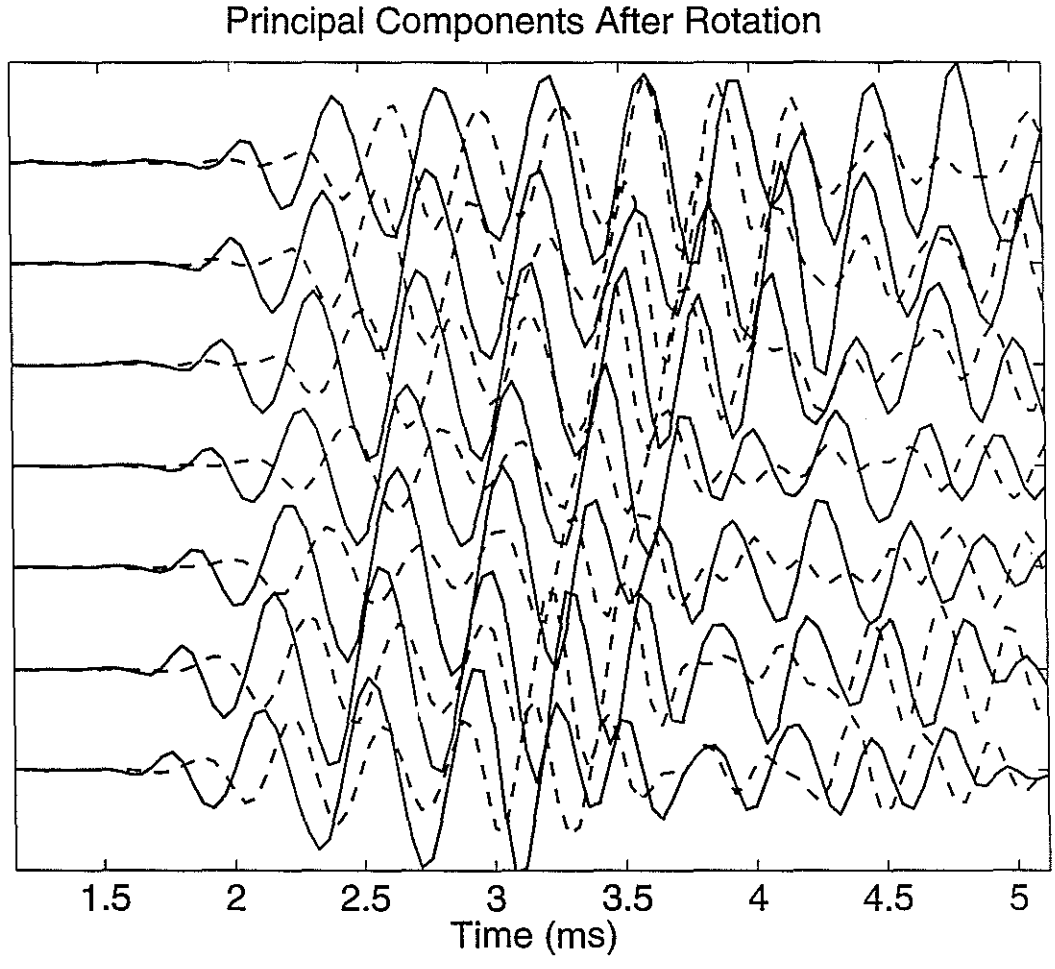

Figure 4: Seismograms on fast (solid lines) and slow (dashed lines) components for a source depth of 3.525 km.

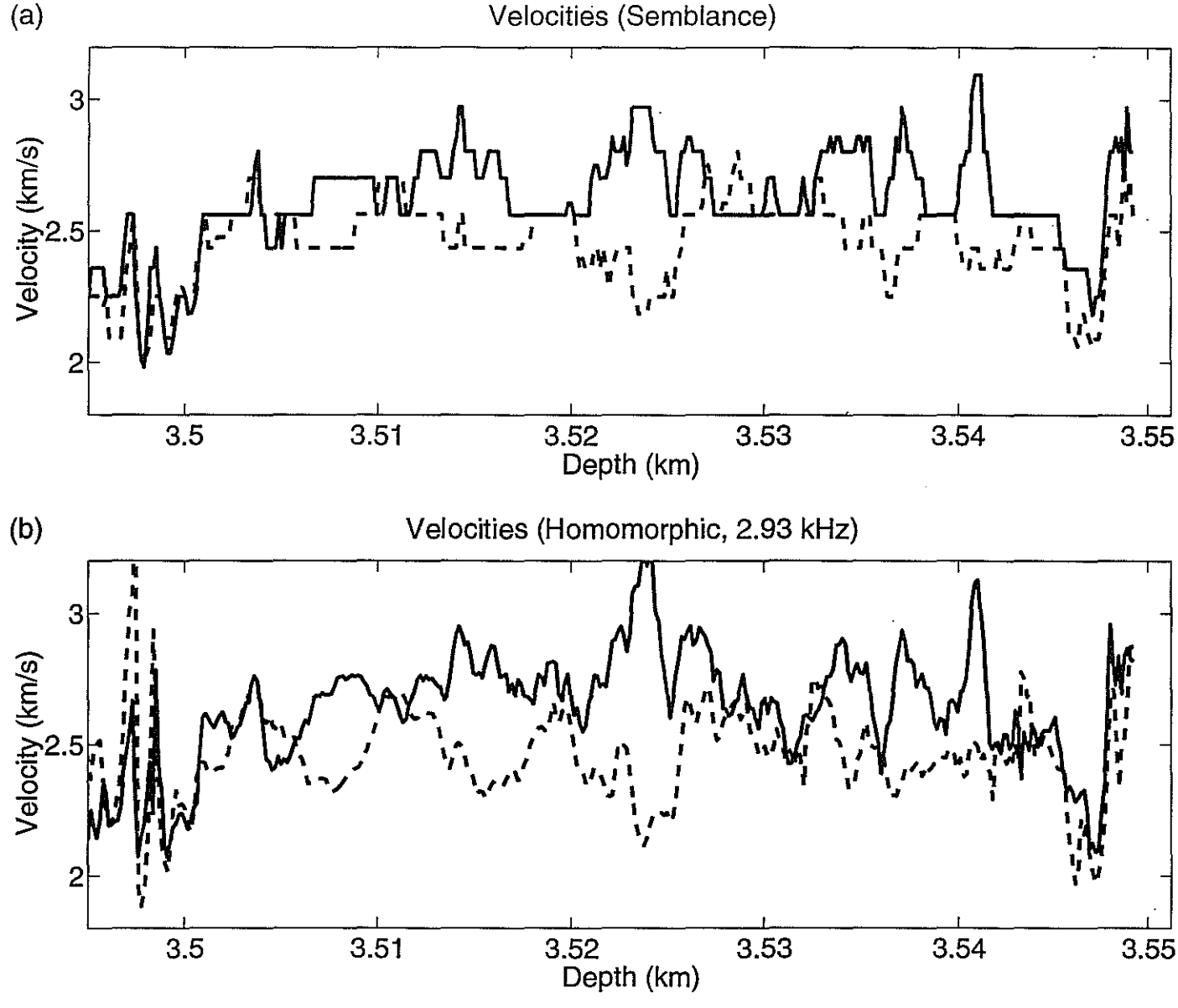

Figure 5: (a) Velocities of fast (solid) and slow (dashed) waves computed with semblance method; (b) velocities computed with homomorphic processing at frequency $\nu = 2.93$ kHz.

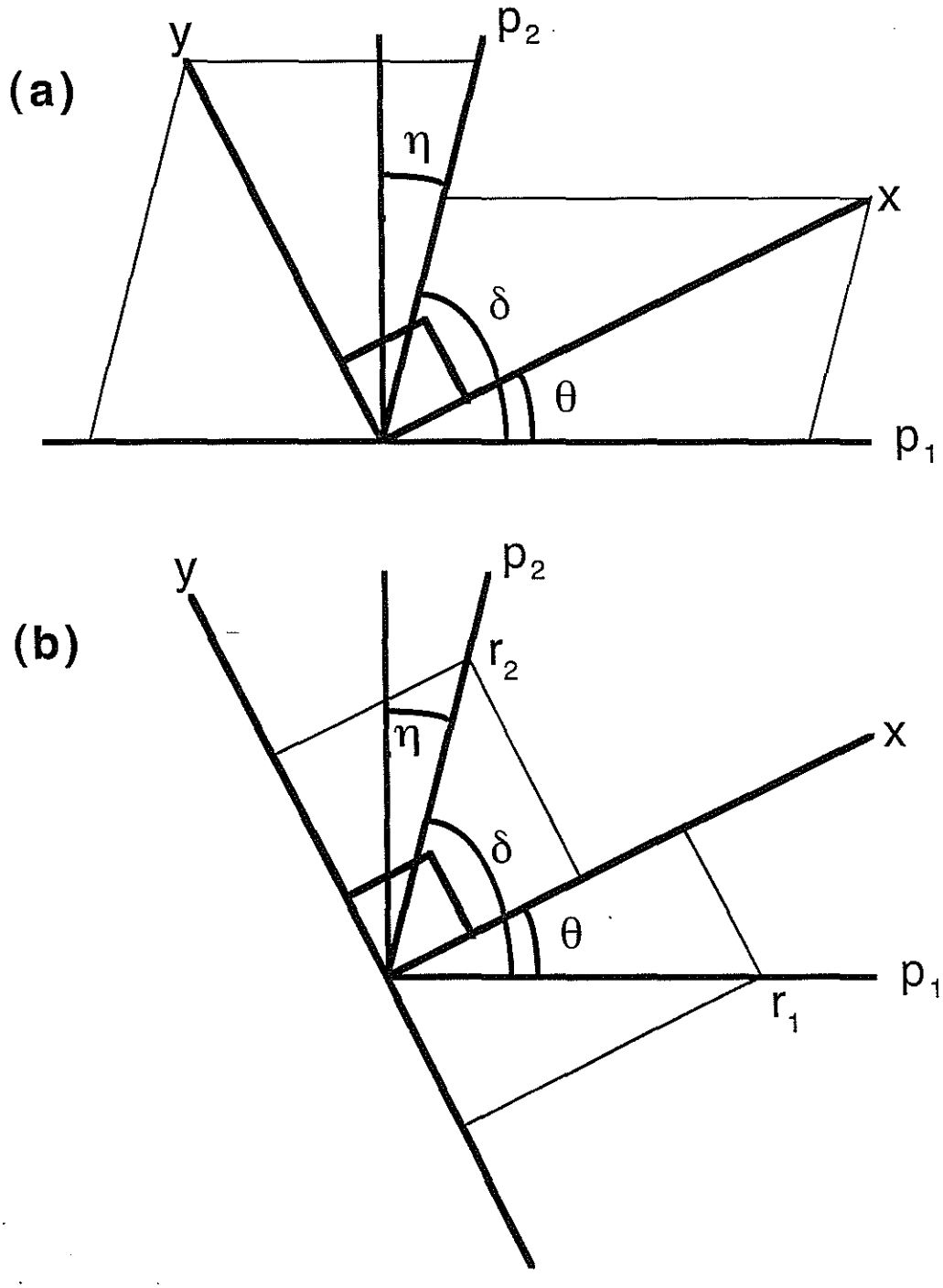

Figure A-1: (a) Projection of x-source and y-source onto principal directions $\hat{p}_1$ and $\hat{p}_2$; (b) projection of vectors r_1 and r_2 on the principal axes onto the x- and y-axes;